

Isospin character of low-lying states in ^{56}Fe

R. De Leo,^{1,2} H. Akimune,¹ N. Blasi,³ I. Daito,¹ Y. Fujita,⁴ M. Fujiwara,¹ S. I. Hayakawa,⁵ S. Hatori,⁶ K. Hosono,¹ H. Ikegami,¹ T. Inomata,¹ I. Katayama,¹ K. Katori,⁷ L. Lagamba,² S. Micheletti,³ S. Morinobu,¹ T. Nakagawa,⁸ S. Nakayama,⁹ A. Narita,⁸ T. Noro,¹ R. Perrino,¹⁰ M. Pignatelli,³ H. Sakaguchi,⁶ J. Takamatsu,^{7,*} A. Tamii,⁶ K. Tamura,¹ M. Tanaka,¹¹ A. Terakawa,⁸ T. Tohei,⁸ M. Tosaki,¹² T. Yamagata,¹³ A. Yamagoshi,⁶ M. Yosimura,⁶ and M. Yosoi⁶

¹Research Center for Nuclear Physics, Osaka University, Osaka 567, Japan

²Dipartimento di Fisica dell' Università and Sezione INFN, via Amendola 173, I-70126 Bari, Italy

³Dipartimento di Fisica dell' Università and Sezione INFN, via Celoria 16, I-20133 Milano, Italy

⁴College of General Education, Osaka University, Osaka 567, Japan

⁵Ashikaga Institute of Technology, Ashikaga, Tochigi 326, Japan

⁶Department of Physics, Kyoto University, Kyoto 606, Japan

⁷Department of Physics, Osaka University, Osaka 567, Japan

⁸Department of Physics, Tohoku University, Sendai 980, Japan

⁹Tokushima University, Tokushima 770, Japan

¹⁰Sezione INFN, via Arnesano, I-73100 Lecce, Italy

¹¹Kobe Tokiwa Junior College, Kobe 653, Japan

¹²Laboratory of Applied Physics, Kyoto Prefectural University, Kyoto 606, Japan

¹³Department of Physics, Konan University, Kobe 658, Japan

(Received 30 January 1996)

Low-lying states in ^{56}Fe , up to an excitation energy of about 4 MeV, have been investigated by means of inelastic proton and deuteron scattering experiments at $E_p=65$ and 400 MeV and at $E_d=56$ MeV, respectively. Measured cross sections and analyzing powers have been compared with coupled-channels calculations using collective form factors; calculations in both the Schrödinger and Dirac formalisms have been carried out for the proton data. For each probe, the matrix elements have been deduced for transitions from the ground state and from the 2_1^+ state to six quadrupole (2^+) states to one octupole (3_1^-) and two hexadecapole (4_1^+ and 4_2^+) states. The obtained matrix elements and the previous values from γ decay or electron inelastic scattering have been used to evaluate the isospin character of the transitions. To discuss the quadrupole mixed-symmetry states in ^{56}Fe , the deduced neutron (M_n) and proton (M_p) components of the matrix elements, or equivalently the isoscalar (M_s) and isovector (M_v) parts, have been compared with theoretical calculations based on the neutron-proton interacting boson model and on the shell model evaluated in a full f - p configuration space. [S0556-2813(96)04006-X]

PACS number(s): 27.40.+z, 21.10.Hw, 25.40.Ep, 25.45.De

I. INTRODUCTION

The experimental determination of the isospin character of nuclear transitions, namely, the evaluation of the neutron (M_n) and proton (M_p) transition matrix elements, can be used more effectively than the total matrix elements (M) to test nuclear structure calculations.

Bernstein *et al.* [1] determined the ratio M_n/M_p for the first 2_1^+ states in closed single-shell nuclei, and showed that proton (neutron) closed shell nuclei have M_n/M_p greater (lesser) than N/Z . Collective excitations with equal contributions from neutrons and protons are isoscalar in character, with a ratio M_n/M_p very near to the N/Z value.

The determination of $M_{n,p}$ for the transitions to the 2^+ levels can add important information on the quadrupole mixed-symmetry (ms) [2] or scissor state (2_{ms}^+) predicted by the neutron-proton interacting boson model (IBA-2) [3], and which correspond to the out-of-phase motion of part of the neutrons against part of the protons.

The presence of mixed-symmetry states in vibrational $A \approx 100$ nuclei has been suggested [4] from the comparison of proton and deuteron data measured at nearly the same bombarding energy per nucleon (E/A).

In the past, two experimental results supported the presence of such theoretically predicted 2^+ states in ^{56}Fe . From the detection of an enhanced magnetic dipole transition in the γ decay of low-lying 2^+ levels towards the 2_1^+ state, Eid *et al.* [5] suggested that the lowest quadrupole mixed-symmetry strength in ^{56}Fe is shared almost equally by the 2_2^+ and 2_3^+ states located at 2.657 and 2.960 MeV of excitation energy, respectively. Similar conclusions have been drawn by Hartung *et al.* [6] through the measurement of inelastic electron scattering.

A slightly different result has been predicted by Nakada *et al.* [7] through the inspection of the wave functions of the 2^+ states in ^{56}Fe evaluated in a large-scale shell-model calculation [8]. They concluded that the 2_2^+ state at 2.657 MeV and the 2_4^+ state at 3.370 MeV share a large fraction of the mixed-symmetry strength.

In this paper, we report a determination of the transition matrix elements M_n and M_p for the first six most strongly

*Present address: Toshiba ULSI Laboratory, Kawasaki 210, Japan.

excited quadrupole (2^+) states, for one octupole (3_1^-) state and for two hexadecapole (4_1^+ and 4_2^+) states in ^{56}Fe . For this purpose, we present the results of three high-resolution inelastic scattering experiments on ^{56}Fe , two taken with polarized proton beams at bombarding energies of 65 and 400 MeV, respectively, and one with deuterons at 56 MeV. Since a complete measurement of the γ decay among the low-lying 2^+ levels in ^{56}Fe is available [9], it is possible to evaluate M_n and M_p from four probes. The same is possible for the 3_1^- state by considering the results from (e, e') scattering [10]. This reduces the uncertainties intrinsic in the use of only two probes.

Our determination of M_n and M_p for the six excited 2^+ states in ^{56}Fe can supply a stringent test for two theoretical calculations available in the literature for ^{56}Fe in the framework of the shell model by Nakada *et al.* [8] and of the IBA-2 model by Rikovska and Stone [11].

To deduce transition matrix elements from the inelastic scattering of hadrons two points must be considered. The first is the experimental requirement of high-energy resolution, which is only available with the use of a magnetic spectrograph, to resolve states at higher excitation energies. Recently, making advantage of high-resolution, Pignatelli *et al.* determined [12,13] the isospin character of many excitations at low energies in some $A \approx 100$ nuclei [12] and in the Nd isotopes [13]. The second concerns coupled-channels (CC) analyses, in which the number of channels to be included in the calculations and the use of transition potentials derived from a folding procedure should be treated with special caution. Only for states with a low multipolarity and a strong collective strength is it sufficient to use [14] a reduced CC scheme which includes two-step transitions through the most relevant states, such as the 2_1^+ and 3_1^- states, and simple transition potentials obtained by deforming [deformed optical potential (DOP)] the optical model (OM) potential.

Some other uncertainties in deducing M_n/M_p have been found [15] for the values extracted from the 400 MeV proton data. For this reason the proton data at the two bombarding proton energies have been analyzed in the present work both in the Schrödinger and in the Dirac formalisms.

II. EXPERIMENTAL METHOD AND RESULTS

The inelastic scattering experiments were performed at the Research Center for Nuclear Physics (RCNP) in Osaka.

Beams of 65 MeV polarized protons and of 56 MeV deuterons were extracted from the AVF cyclotron. The proton beam polarization was around 70% and its intensity was about 12 nA. The deuteron beam intensity was kept around 60 nA. The target used was a self-supporting ^{56}Fe foil with a thickness of 1.05 mg/cm^2 and an isotopic enrichment greater than 99%. Scattered particles were analyzed by using the magnetic spectrograph ‘‘Raiden’’ [16] and were detected by a two-dimensional position-sensitive proportional counter system [17]. To maximize the energy resolution, the solid angle of the spectrograph was set to be 3.2 msr and the kinematic line broadening was compensated. A final energy resolution of about 30 keV full width at half maximum (FWHM) was obtained for both particles. An example of the obtained energy spectra is reported in Fig. 1 of Ref. [18] for both particle beams. Most of the relevant excited states up to

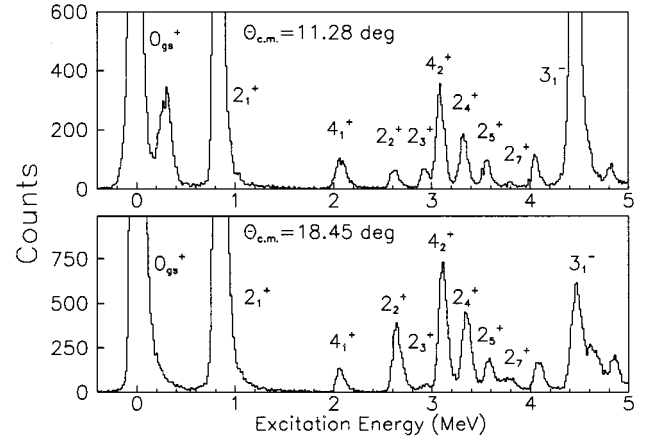


FIG. 1. Energy spectra for the inelastic scattering of 400 MeV protons at the scattering angles of 11.28° and 18.45° . The states analyzed in this paper are indicated. Different relative yields are observed for the 2_3^+ state at the two scattering angles compared to those for its neighboring 2_2^+ and 2_4^+ states.

the 3_1^- level at $E_x=4.510 \text{ MeV}$ have been analyzed in this paper. Following the energy scheme of ^{56}Fe in Ref. [9], we identified the peaks corresponding to the ground state ($0_{g.s.}^+$), six 2^+ states at $E_x=0.846, 2.657, 2.960, 3.370, 3.602,$ and 3.832 MeV , the 3_1^- state, and two 4^+ states at $E_x=2.085$ and 3.123 MeV . No appreciable excitation was recognized for the 2_6^+ state reported in Ref. [9] at $E_x=3.748 \text{ MeV}$. The 2_3^+ ($E_x=2.960 \text{ MeV}$) and 2_5^+ ($E_x=3.602 \text{ MeV}$) levels were not separated from their respective neighbors 0_2^+ at $E_x=2.942 \text{ MeV}$ and 0_3^+ at $E_x=3.598 \text{ MeV}$. The same happens for the 2_4^+ ($E_x=3.370 \text{ MeV}$) level, which was not resolved from the 6_1^+ state at $E_x=3.388 \text{ MeV}$. A preliminary analysis of these low-energy experiments has been presented elsewhere [18].

In addition, the (\vec{p}, p') experiment at $E_p=400 \text{ MeV}$ was carried out at the ‘‘new’’ ring cyclotron facility at RCNP. A polarized proton beam produced by an atomic-beam-type ion source was accelerated to 65 MeV with the AVF cyclotron. The beam was injected into the $K=400 \text{ MeV}$ ring cyclotron, and further accelerated to 400 MeV. Beam polarization of around 80% and intensities of about 1 nA were kept during the experiment. The beam extracted from the ring cyclotron was transported to a self-supporting ^{56}Fe target with a thickness of 43 mg/cm^2 (99.9% isotopic enrichment). Scattered protons were analyzed by using the magnetic spectrograph ‘‘Grand Raiden’’ [19] operated with an opening angle of $\pm 8.5 \text{ mrad}$ horizontally and of $\pm 20 \text{ mrad}$ vertically. Its focal-plane counter system consists of two multiwire drift chambers (MWDC’s) [20], each with an effective area of $1150 \text{ mm} \times 45 \text{ mm}$, and two plastic-scintillation counters placed behind the MWDC’s. The MWDC’s have a detection efficiency greater than 99%, and an intrinsic position resolution of $200 \mu\text{m}$. The ray-tracing technique was applied to determine the scattering angles at the target from the arrival positions and incidence angles of scattered protons at the focal plane after particle identification. The available energy resolution was strongly dependent upon the coupling parameters between the two cyclotrons and upon their stability. Energy resolutions of about 40 keV FWHM were obtained

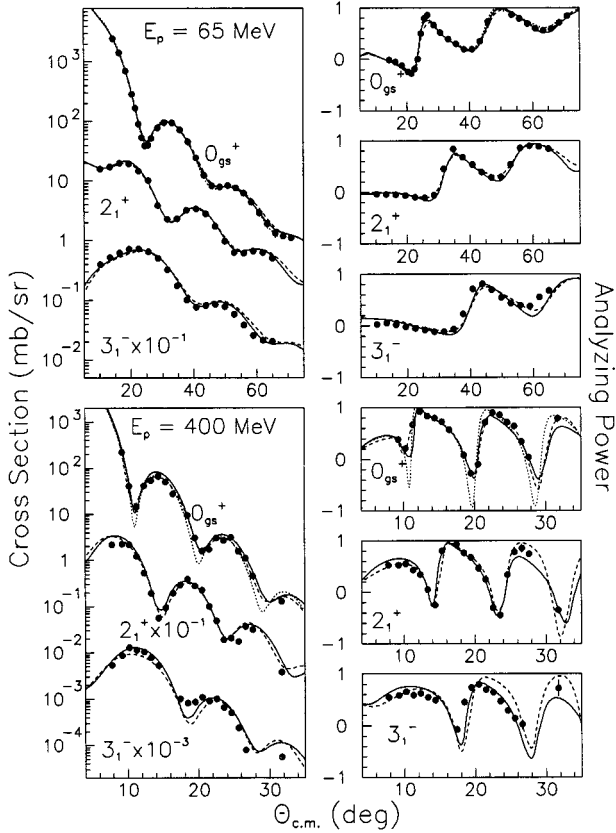


FIG. 2. Differential cross sections (left side) and analyzing powers (right side) for the $0_{g.s.}^+$, 2_1^+ , and 3_1^- states in ^{56}Fe determined in the proton elastic and inelastic scattering at 65 (top part) and 400 (bottom part) MeV. The experimental data are shown by the solid circles. The curves are the results from CC calculations in the Schrödinger (solid line) and Dirac (dashed and dotted lines) formalisms. The solid and dashed curves refer to the OM parameters from Table I. The dotted curves refer to the EDAD-1 potentials in Ref. [22]. The first derivative form factors (δ' FF) are used in all the calculations. The solid curves fitted to the 2_1^+ and 3_1^- cross sections at $E_p=400$ MeV are normalized using a normalization factor of 1.2 (see text).

for only a few hours. Instead, most of the experiment was run with a resolution of about 100 keV. Two examples of energy spectra with good energy resolution are reported in Fig. 1. The 2_3^+ level shows an angular behavior different from that of the 2_2^+ and 2_4^+ levels. Referring to the level scheme of ^{56}Fe , even with 100 keV of energy resolution, the situation of resolving the doublet states analyzed in this paper is not worse compared with that of the two present experiments at lower energies.

The yield of each peak in the spectra was converted into cross sections using the target thickness, the solid angle, and the collected charges. The systematical uncertainty in the normalization factor (UNF) of the experimental cross sections has been estimated to be of the order of 10%. For analyzing powers, this error is much smaller due to the cancellation of these uncertainties. Measured cross sections and analyzing powers for the elastic scattering, for the six 2^+ levels, and for the 3_1^- , 4_1^+ , and 4_2^+ states are presented in Figs. 2–6. The error bars on the data points in the figures represent only statistical errors.

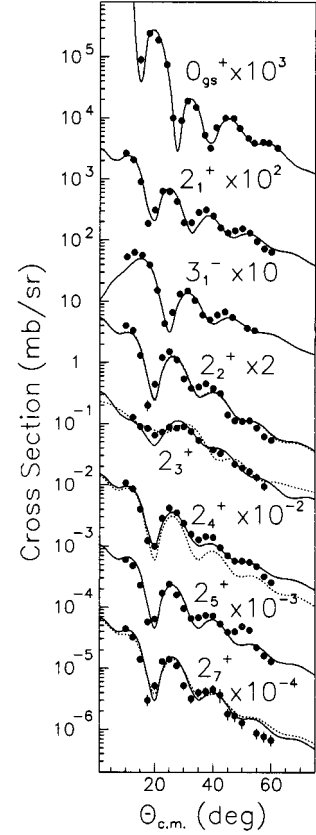


FIG. 3. Differential cross sections for the $0_{g.s.}^+$, 2_1^+ , 3_1^- , and other five 2^+ levels from the deuteron elastic and inelastic scattering at $E_d=56$ MeV. The experimental data are shown by the solid circles. The curves are from the Schrödinger CC calculations with coupling constants from Table II and refer to the $0_{g.s.}^+ - 2_1^+ - 2_i^+$ coupling for the $2_{i>1}^+$ levels, and to the $0_{g.s.}^+ - 2_1^+ - 3_1^-$ coupling for the $0_{g.s.}^+$, 2_1^+ , and 3_1^- levels. The solid curves through the 2_1^+ , 3_1^- , 2_4^+ , and 2_5^+ data are the results of the calculations using δ' FF's. The dotted (solid) curves through the 2_2^+ , 2_3^+ , and 2_7^+ data are the results of the calculations using the δ' FF's (mixed δ' - δ'' FF's). The dotted curve for the 2_4^+ state is obtained by excluding the contribution of the excitation of the unresolved 6_1^+ level.

III. COUPLED-CHANNELS CALCULATIONS

A. Fits of the $0_{g.s.}^+$, 2_1^+ , and 3_1^- data

Both the CC and the DOP model have been used to evaluate the coupling constants (β) of the direct and two-step excitations. The calculations have been carried out by using the code ECIS88 [21].

Hintz *et al.* [15] used the Schrödinger (S) equation and the DOP model to deduce the M_n/M_p ratio in the neighboring nucleus ^{58}Ni from the proton data at bombarding energies around 400 MeV. They found lower M_n/M_p values compared to the results obtained from the data at the bombarding energies below 100 MeV and at 800 MeV. One possible explanation [15] could reside in the strong variation of the shape of the absorption term of the OM potential with the bombarding energy. Its volume term, weaker than the surface one at low bombarding energies, becomes dominant at high energies and is determined from the elastic scattering. At $E_p=400$ MeV, the elastic scattering is sensitive to the inner part of the nucleus, while inelastic scattering is still

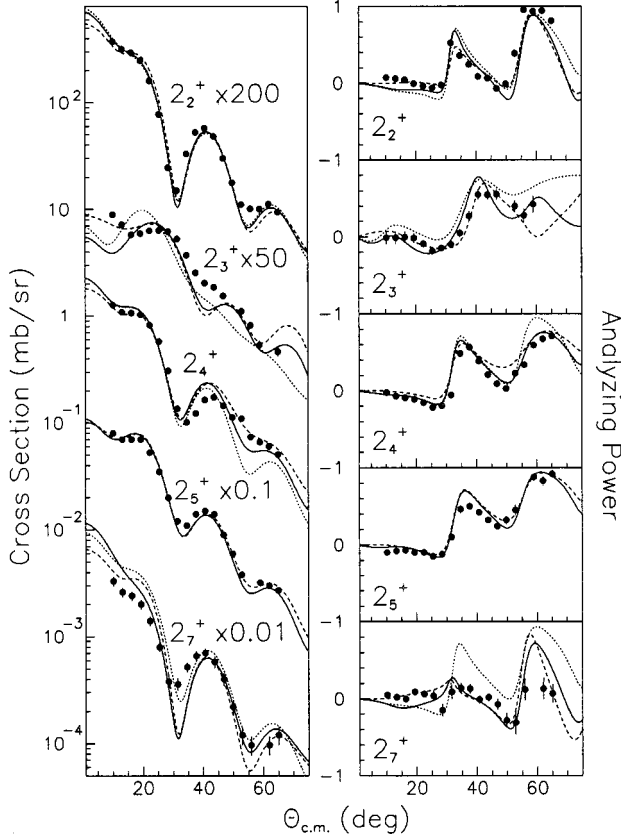


FIG. 4. Differential cross sections (left part) and analyzing powers (right part) for five 2^+ states in ^{56}Fe determined in the inelastic proton scattering at $E_p=65$ MeV. The experimental data are shown by the solid circles. The curves are obtained from the CC calculations in the Schrödinger (solid and dotted lines) and Dirac (dashed line) formalisms. The dotted curves through the 2_2^+ , 2_3^+ , and 2_7^+ data are obtained using δ' FF's, and the solid and dashed curves are the results obtained by taking into account a δ' - δ'' mixing. All the curves through the data of the 2_4^+ and 2_5^+ states are obtained using δ' FF's. The solid and dashed curves through the data of the 2_4^+ state include a contribution due to the excitation of the unresolved 6_1^+ level.

sensitive to the nuclear surface through the surface peaking of the transition potentials. Therefore, the use of a volume absorption potential for analyzing the inelastic scattering data at 400 MeV could lead to incorrect M_n/M_p values.

These marked changes in the shapes of the potentials do not appear in the Dirac (D) formalism. In fact, potentials derived [22] in this formalism vary slowly without any large dependence on target mass (from ^{12}C to ^{208}Pb) or bombarding energy (in the range 20–1040 MeV). At present, the Dirac OM potentials are used to reproduce [23] the proton inelastic scattering data to the same extent as the Schrödinger potentials. For this reason, as well as to compare results from the two methods, the 65 and 400 MeV proton data have been analyzed in this work both within the S and the D formalisms.

In this work, we confine our studies to the excitation of low-spin states excited by only light-mass projectiles. Therefore, we do not expect [14] appreciable anomalies in the M_n/M_p values extracted in this paper by using the DOP model.

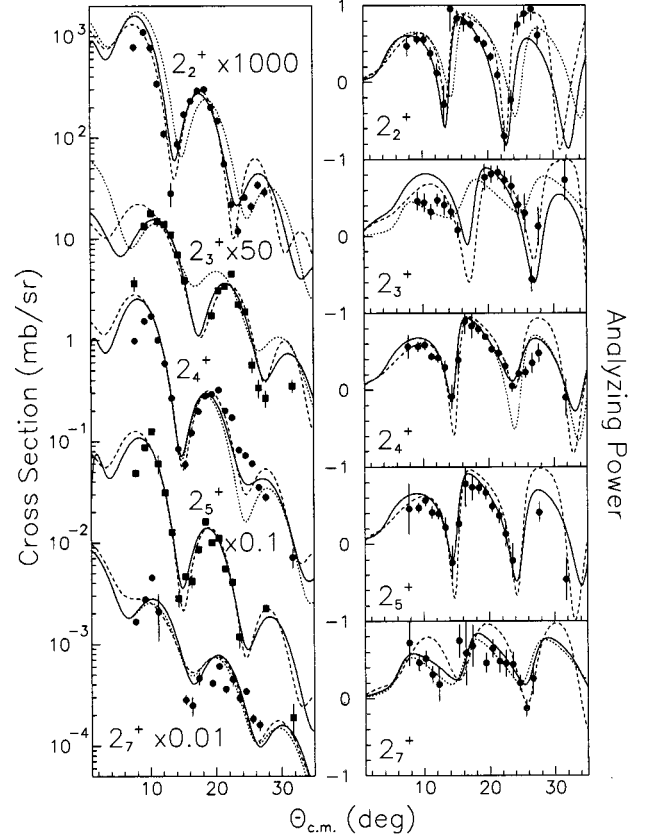


FIG. 5. Differential cross sections (right) and analyzing powers (left part) for the five 2^+ states in ^{56}Fe determined in the inelastic proton scattering at $E_p=400$ MeV. The explanations of symbols and lines are the same as in Fig. 4. The absolute magnitudes of the solid and dotted curves given by the Schrödinger calculations have been decreased by a factor of 1.2 (see text).

To reduce uncertainties in the OM parameters, we searched for new OM parameter sets in a CC scheme in which the $0_{g.s.}^+$ state was coupled to the strongly excited 2_1^+ and 3_1^- levels. The inclusion of these two levels is of particular importance for the imaginary potentials which are affected by CC effects and influence the extraction of coupling constants. We used first derivative (δ') form factors (FF's) and searched for the β values of the $0_{g.s.}^+-2_1^+$ and $0_{g.s.}^+-3_1^-$ transitions, and of the $2_1^+-2_1^+$ reorientation terms. No link between the two quadrupole β 's was made in these searches. In fact, Ballester *et al.*, [24] in the analysis of a $^{56}\text{Fe}(\alpha, \alpha')$ experiment, showed that both the asymmetric-rotor and the harmonic-vibrational models give similar results for the fits of the $0_{g.s.}^+$ and 2_1^+ cross sections. In the first-order approximation, the reorientation term due to the $2_1^+-2_1^+$ transition is small and is neglected in both models.

The starting values for the proton Schrödinger OM parameters at 65 MeV were taken from the systematic parameters given by Noro *et al.* [25]. The calculations with these parameters underestimated the elastic cross section by about 10%. The final parameter values listed in Table I minimize the chi-square (χ^2) value for fitting the cross sections and analyzing powers of the $0_{g.s.}^+$, 2_1^+ , and 3_1^- states without renormalization factors (NF=1.0). The results are shown by the solid lines in Fig. 2. They differ from those of Ref. [25]

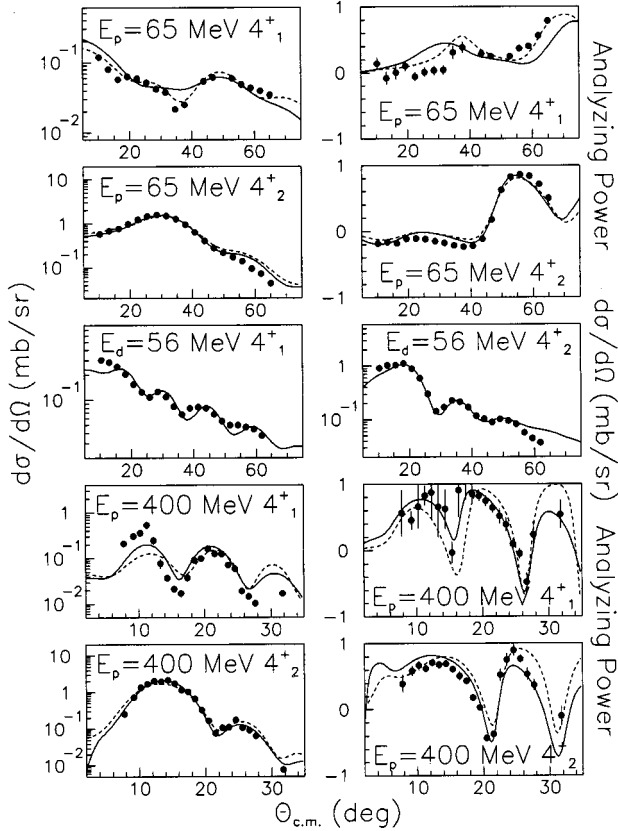


FIG. 6. Cross sections and analyzing powers for the 4_1^+ and 4_2^+ states in ^{56}Fe determined in scattering of 65 MeV polarized protons (upper four parts), 400 MeV polarized protons (lower four), and 56 MeV deuterons (central two). The solid and dashed curves are the results of the Schrödinger and Dirac calculations, respectively.

only in the depth and radius of the volume imaginary potential. The error (4%) on NF reported in Table I is an estimation of the uncertainty in normalizing theory to experiment and it has been used to get the uncertainties of the transition matrix elements. The extracted β values are presented in Table II.

For the analysis of the deuteron data, the initial OM parameters were taken from the mass-energy nonrelativistic systematics of Daehnick *et al.* [26]. Also, in the deuteron case, the final values (Table I) do not require a renormalization of the experimental data. The obtained fits are shown in the upper part of Fig. 3.

In the framework of the Schrödinger equation, no OM parameter set was available for proton scattering data on ^{56}Fe at $E_p=400$ MeV. The parameter search was started from the SN set of Ref. [15] obtained from $^{58}\text{Ni}(p,p')$ data at $E_p=333$ MeV. To operate the ECIS88 code at 400 MeV, we used relativistic kinematics and we included 100 partial waves in the calculations. In the initial stage of the present analysis, it was found that a renormalization of cross sections was necessary to minimize, with the same OM parameter set, the χ^2 values of both the $0_{\text{g.s.}}^+$ cross section and analyzing power data. A good fit could only be achieved with a NF value increased to 1.2. The obtained final set minimizes also the χ^2 values of the 2_1^+ and 3_1^- data (see Table I). The results are shown in the lower part of Fig. 2 as solid lines.

The obtained β values are listed in Table II. We checked the validity of the adopted OM parameters in other searches which gave similar χ^2 and NF values in spite of different initial sets (P1 and P2 in Ref. [15]). The obtained NF value, well beyond our UNF estimation (10%), is similar to those reported by Jones *et al.* [27] in the Schrödinger DOP analysis for the inelastic scattering of polarized protons from ^{12}C at $E_p=200-700$ MeV.

The Dirac formalism does not require any renormalization to fit the 400 MeV experimental cross sections. The results are compared in Fig. 2 where the dotted lines represent the fits to the 400 MeV elastic channel data evaluated with the average potentials EDAD-1 (energy-dependent, A-dependent) of Ref. [22]. The dashed lines in Fig. 2 represent a fit to the proton data with the D potentials. As discussed in Ref. [22], only the scalar and vector, both real and imaginary, and Coulomb potentials have been considered. The tensor terms are neglected. The D potentials obtained at the two bombarding proton energies are listed in Table I. The shapes of their Schrödinger-equivalent potentials are presented in Fig. 7. Only the real potential shows a somewhat different shape at the two energies (see the solid and dashed lines in Fig. 7 for 65 and 400 MeV protons, respectively).

The volume integrals of the different potentials and their radial moments for the δ' and δ'' form factors are reported in the second part of Table I. For the proton probe, the W_v imaginary part is the dominant term of the S potential at 400 MeV. The radial ratio $\int W_{v,\text{tr}}(r, \delta') r^2 d\tau / \int W_v(r) d\tau$ is, however, nearly 50% lower than that of the dominant real (V_0) potential at 65 MeV. The real scalar (V_0) and vector (V_s) terms are dominant in the D potential. Their radial ratios are nearly constant at the two proton energies.

The resulting β 's from these searches for the excitation of the 2_1^+ and 3_1^- levels have been reported in the first lines of Table II. In particular, the direct coupling constant for the 2_1^+ level has an opposite sign with respect to its reorientation term, indicating a prolate shape for ^{56}Fe , as found in Ref. [24].

B. Results of CC analyses of higher 2^+ levels

The vibrational model predicts that, in presence of anharmonicities and other effects, the $E2$ - $E2$ two-phonon quadrupole excitations can be split [28] over many 2^+ states and mixed with other configurations. A fragmentation of the two-phonon component is also predicted by the quasiparticle phonon model (QPM) [29] and has been observed in the Nd isotopes [13]. In addition, many of the 2_i^+ states analyzed in the present work are linked by γ decay [9]; a complete CC scheme may require one to include all the γ -connected states.

A test result to examine the amount of two-step contributions to the cross section and analyzing power of a 2_i^+ state at $E_x=3$ MeV is reported in the top and middle parts of Fig. 8 for the cases of inelastic proton scattering at 65 and 400 MeV, respectively. The same coupling constants have been used at the two energies. The solid curves represent the direct excitation of this 2_i^+ state from the $0_{\text{g.s.}}^+$ state with a δ' transition FF. The dotted lines show the contribution of the two-step (indirect) excitation via the 2_1^+ state. The significant differences between these lines delineate the sensi-

TABLE I. Schrödinger (S) and Dirac (D) optical model parameters (depths in MeV, lengths in fm) used in the CC calculations described in the text for the three p , d , and p_{400} probes. The signs of the potentials (Woods-Saxon shapes) are as used in the code ECIS88 [21] in the “external form factor model.” In the Dirac formalism the potentials are scalar real (V_0) and imaginary (W_v), vector real (V_s) and imaginary ($W_{s,i}$), and tensor real (V_{s0}) and imaginary ($W_{s0,i}$). The renormalization factors of experimental cross sections required by these OM potentials are denoted as NF. Numbers in parentheses indicate the estimated errors and refer to the last decimals of the value. In the middle part, the volume integrals of the different potentials (in units of 10^3 MeV fm^3) and of the quadrupole moments of their δ' and δ'' FF (in units of 10^3 MeV fm^5) are reported. In the lower part, their relative multipole matrix elements in units of the coupling constant [see Eq. (1)] are given (in $e \text{ fm}^\lambda$).

	P_S	d_S	$P_{400,S}$	P_D	$P_{400,D}$
V_0	36.09	78.7	22.16	-438.5	-335.9
r_0	1.190	1.180	0.980	1.045	1.044
a_0	0.726	0.784	0.845	0.635	0.646
W_v	8.36	7.95	60.80	11.88	2.33
r_v	1.127	1.486	0.918	1.206	1.565
a_v	0.729	1.014	0.664	0.308	0.220
V_s	0.0	0.0	0.0	338.1	248.0
$r_{v,s}$				1.056	1.038
$a_{v,s}$				0.606	0.614
W_s	3.28	4.014	0.0	-21.14	-40.14
r_s	1.349	1.452		1.216	1.060
a_s	0.459	0.618		0.638	0.721
V_{s0}	5.99	3.58	0.832	0.0	0.0
$r_{v,s0}$	1.073	1.125	1.172		
$a_{v,s0}$	0.621	0.448	0.665		
W_{s0}			-3.45	0.0	0.0
r_{ws0}			0.984		
a_{ws0}			0.655		
r_c	1.3	1.4	1.2	1.2	1.2
NF	1.00(4)	1.00(4)	1.20(7)	1.00(4)	1.00(7)
$\int V_0(r)d\tau$	17.84	39.56	7.35	-146.5	-112.8
$\int V_{0,\text{tr}}(r,\delta')r^2d\tau$	108.1	241.5	34.80	-684.2	-528.4
$\int V_{0,\text{tr}}(r,\delta'')r^2d\tau$	176.3	383.1	49.33	-1119	-859.3
$\int W_v(r)d\tau$	3.60	8.04	14.93	5.10	2.12
$\int W_{v,\text{tr}}(r,\delta')r^2d\tau$	19.95	79.03	57.30	27.05	18.41
$\int W_{v,\text{tr}}(r,\delta'')r^2d\tau$	31.95	124.08	87.92	51.88	36.34
$\int V_s(r)d\tau$	0.0	0.0	0.0	114.1	80.41
$\int V_{s,\text{tr}}(r,\delta')r^2d\tau$	0.0	0.0	0.0	534.0	366.9
$\int V_{s,\text{tr}}(r,\delta'')r^2d\tau$	0.0	0.0	0.0	889.5	605.5
$\int W_s(r)d\tau$	2.07	4.00	0.0	-10.56	-14.71
$\int W_{s,\text{tr}}(r,\delta')r^2d\tau$	18.46	42.41	0.0	-63.92	-73.50
$\int W_{s,\text{tr}}(r,\delta'')r^2d\tau$	26.35	59.00	0.0	-109.3	-115.5
$M(E2,\delta')/\beta$	174.5	197.7	115.7	138.3	134.8
$M(E2,\delta'')/\beta$	279.8	308.3	172.5	212.4	207.3
$M(E3,\delta')/\beta$	1048	1310	606.0	726.1	733.6
$M(E3,\delta'')/\beta$	2005	2417	1042	1404	1309
$M(E4,\delta')/\beta$	6604	9278	3445	4025	4266
$M(E4,\delta'')/\beta$	14489	19476	6564	8830	8498

tivity of calculations in estimating direct and two-step processes in the data. The differential cross sections for the direct excitation are more oscillating than those for two-step contributions. In search procedures this will result in smaller correlation errors for the direct contributions. The oscillation pattern of the direct excitation increases with increasing the bombarding energy from 65 to 400 MeV. The indirect contribution becomes relatively stronger, slightly exceeding the minima of the direct one, indicating that two-step processes are important for a correct description of the inelastic proton scattering even at 400 MeV.

The 2_i^+ reorientation term and the contributions from other 2^+ states (not shown in the figure) are smaller and have angular distributions very similar to the dominant $2_1^+-2_i^+$ term shown by the dotted curves. These contributions were not included in the search because of their indistinguishability from the $2_1^+-2_i^+$ term. Thus, the $2_1^+-2_i^+$ β 's extracted in the present analyses will include all these contributions and should be treated as effective β values.

In addition, as shown by Ballester *et al.*, [24] ^{56}Fe displays a hexadecapole vibration mode which affects primarily states with $J^\pi=4^+$ and 6^+ , and, to a lesser extent, also the $J^\pi=2^+$ ones. This $2_1^+-2_i^+$, $L=4$ contribution is shown with the dot-dashed lines in Fig. 8. It is very similar to the $4_1^+-2_i^+$, $L=2$ contribution, which is not reported here.

The major uncertainty in the fits of the data for the higher 2^+ levels comes from the ambiguities in determining the radial shape of form factors. These levels are not always completely collective and reproduced by a surface-peaked δ' FF. In particular cases [4,12,13], better fits are obtained by a mixing of δ' and δ'' FF's. This mixing is also suggested by the vibrational model, in which second-order couplings are assumed [28] as a δ'' FF. Similarly the IBA model assumes [30] a δ'' FF for the part of the transitions conserving the number of d bosons.

Differences in cross sections and analyzing powers produced by δ' and δ'' FF's (dashed lines) can be seen in the upper parts of Fig. 8 for 65 and 400 MeV protons, respectively. The latter have been evaluated with a coupling constant reduced by a factor of 20 compared to that of the solid curves. The cross sections and analyzing powers of the two contributions tend to go out of phase at backward angles.

In general, in the analysis of these $2_{i>1}^+$ data, first we have considered a “simple” CC scheme with only three ($0_{\text{g.s.}}^+$, 2_1^+ , and 2_i^+) states, $L=2$ transitions, and without the $2_i^+-2_i^+$ reorientation term. We searched for the β 's of the two $0_{\text{g.s.}}^+-2_i^+$ and $2_1^+-2_i^+$ transitions, keeping the $0_{\text{g.s.}}^+-2_1^+$ and $2_1^+-2_1^+$ terms fixed at the values from the previous analysis. When any of the three probe data was not sufficiently reproduced, we added a δ'' FF to the direct excitation, or introduced other coupled channels. We did not include the δ'' FF in two-step transitions because of their large uncertainties. The final CC scheme should give acceptable fits for the experimental data of all the three probes, and the β values for corresponding transitions should be consistent.

The final CC fits for the higher five 2^+ states in ^{56}Fe are reported in Figs. 3–6 for both the S and D formalisms. The extracted coupling constants are listed in Table II with uncertainties which include only the correlation errors.

TABLE II. Coupling constants (β_λ) corresponding to the lowest possible multipoles ($\lambda \geq 2$) for the indicated transitions and for the three probes (p , d , p_{400}), deduced from the CC calculations described in the text. The S and D symbols refer to the Schrödinger and Dirac calculations, respectively. Numbers in parentheses are the correlation errors resulting from CC calculations. The signs of the parameters are those used in ECIS88 [21] in the “external form factor model.”

$J_{\text{in}}^\pi - J_{\text{fin}}^\pi$	$\beta^{(p_s)}$	$\beta^{(d_s)}$	$\beta^{(p_{400,s})}$	$\beta^{(p_D)}$	$\beta^{(p_{400,D})}$
$0_{\text{g.s.}}^+ - 2_1^+$	-0.218(7)	-0.183(11)	-0.248(26)	-0.271(7)	-0.255(16)
$2_1^+ - 2_1^+$	0.185(67)	0.182(80)	0.220(120)	0.225(70)	0.202(91)
$0_{\text{g.s.}}^+ - 3_1^-$	-0.156(9)	-0.108(6)	-0.206(12)	-0.190(10)	-0.196(14)
$0_{\text{g.s.}}^+ - 2_2^+$	-0.049(3)	-0.036(4)	-0.030(6)	-0.049(2)	-0.032(6)
$0_{\text{g.s.}}^+ - 2_2^+{}^a$	-0.006(3)	-0.003(4)	-0.016(2)	-0.012(2)	-0.015(2)
$2_1^+ - 2_2^+$	-0.259(21)	-0.180(52)	-0.269(114)	-0.177(50)	-0.252(79)
$0_{\text{g.s.}}^+ - 2_3^+$	-0.029(2)	-0.020(3)	-0.066(6)	-0.047(2)	-0.053(3)
$0_{\text{g.s.}}^+ - 2_3^+{}^a$	0.011(2)	0.009(1)	0.023(2)	0.019(2)	0.014(1)
$2_1^+ - 2_3^+$	0.122(41)	0.088(45)	0.108(67)	0.070(46)	0.102(48)
$0_{\text{g.s.}}^+ - 2_4^+$	-0.051(4)	-0.031(3)	-0.075(5)	-0.060(2)	-0.076(6)
$2_1^+ - 2_4^+$	-0.073(30)	-0.070(38)	-0.100(65)	-0.092(42)	-0.120(102)
$2_1^+ - 6_1^+$	-0.28(7)	-0.20(5)	-0.40(10)	-0.40(10)	-0.40(10)
$0_{\text{g.s.}}^+ - 2_5^+$	-0.045(2)	-0.028(3)	-0.052(6)	-0.052(2)	-0.052(4)
$2_1^+ - 2_5^+$	-0.040(25)	-0.043(30)	-0.102(81)	-0.053(25)	-0.072(80)
$0_{\text{g.s.}}^+ - 2_7^+$	-0.019(4)	-0.024(3)	-0.023(5)	-0.013(4)	-0.023(5)
$0_{\text{g.s.}}^+ - 2_7^+{}^a$	-0.004(2)	0.002(1)	0.004(3)	-0.014(2)	0.004(3)
$2_1^+ - 2_7^+$	-0.202(120)	-0.063(27)	-0.661(142)	-0.102(60)	-0.691(148)
$0_{\text{g.s.}}^+ - 4_1^+{}^a$	-0.016(4)	-0.011(2)	-0.022(3)	-0.021(3)	-0.020(3)
$2_1^+ - 4_1^+$	0.451(121)	0.313(22)	0.582(71)	0.472(49)	0.714(116)
$0_{\text{g.s.}}^+ - 4_2^+$	-0.088(5)	-0.053(5)	-0.118(6)	-0.109(5)	-0.110(7)

^aSecond derivative form factor.

With the simplified scheme, the calculations for both cross sections and analyzing powers of the 2_2^+ level are partly out of phase with respect to the experimental data especially for 400 MeV protons (see the dotted lines in Figs. 3–5 where only the S calculations are reported). Attempts to improve the fits with the inclusion of a 4^+ level or a $L=4$, $2_1^+ - 2_2^+$ contribution in the CC scheme were not successful. An improvement was instead achieved by including a δ'' FF

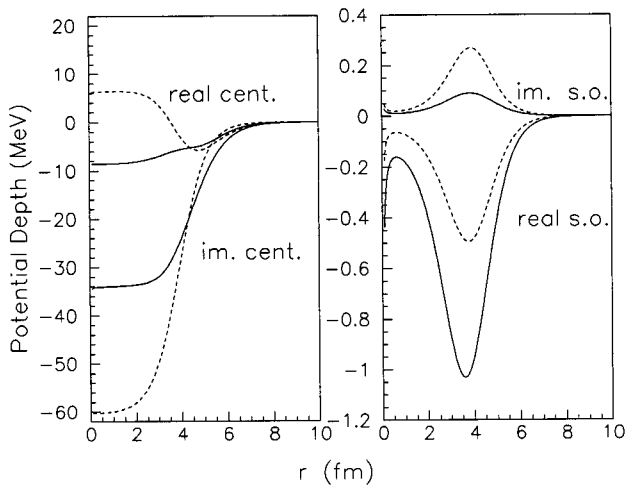


FIG. 7. Schrödinger equivalent of the Dirac potentials of Table I. The real and imaginary central potentials are given on the right side. The spin orbit potentials are shown on the left part of the figure. The solid and dashed lines are the potential shapes for 65 and 400 MeV protons, respectively.

in the direct excitations (see the solid and dashed curves in Figs. 3–5 for the S and D calculations, respectively).

The 2_3^+ state has an angular distribution very different from those of the other 2^+ states. This could be due to the presence of a contribution from the unresolved 0_2^+ level. This state can be a member of the $E2-E2$ two-phonon triplet and therefore strongly excited. A calculation of this indirect contribution, arbitrarily normalized, is reported with the dotted lines in the bottom part of Fig. 8 together with the data of the $0_2^+ - 2_3^+$ doublet (solid circles) at 65 MeV protons. The direct excitation of the 0_2^+ state from the $0_{\text{g.s.}}^+$ has been estimated using Satchler’s surface vibration model [31] and the result is shown by the solid lines. Some improvement in fitting the 0_2^+ cross sections of other nuclei was obtained in Refs. [12,28,32] by folding Satchler’s mass FF with a density-dependent effective interaction. After the folding the resulting transition potentials are quite similar to a δ'' FF. The result of a direct excitation using this FF is shown (arbitrarily normalized) by dashed lines.

The cross sections calculated for the three possible excitations of the 0_2^+ level show oscillation patterns stronger than those of the data. Thus any contribution to the doublet should come from a highly improbable strong destructive interference of these contributions. A similar interference is required by the analyzing powers, since the calculated contributions have large values between 10° and 30° , not observed experimentally.

We therefore assumed that the 0_2^+ level is weakly excited and that the peak at $E_x = 2.942$ MeV is mostly due to the 2_3^+ state. Our assumption is confirmed by the 20 MeV deu-

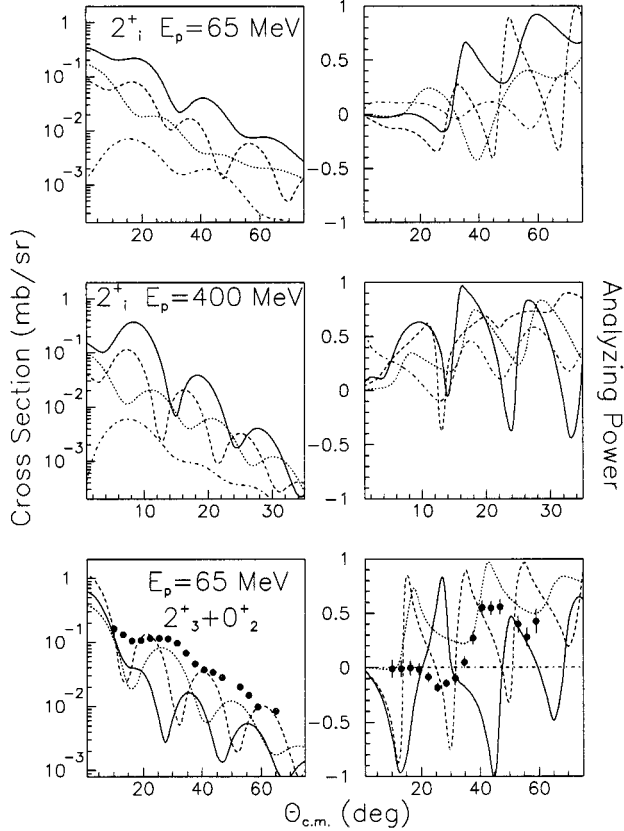


FIG. 8. Calculated cross sections (left side) and analyzing powers (right side) for a 2_1^+ state in ^{56}Fe at $E_x = 3$ MeV, excited by inelastic proton scattering at 65 (top part) and 400 MeV (middle part). In these two parts of the figure, the solid and dashed curves represent the direct (from the $0_{\text{g.s.}}^+$ state) excitation of the 2_1^+ level with the δ' and δ'' form factors, respectively. The dotted and dot-dashed lines are the two-step contributions for excitation via the 2_1^+ state with $L=2$ and $L=4$ angular momenta, respectively. In the bottom part of the figure, the solid points represent the experimental data for the unresolved $2_3^+ - 0_2^+$ doublet at $E_x = 2.960$ MeV and $E_p = 65$ MeV. The curves correspond to the three different calculations: the direct excitation of only the 0_2^+ state, with the Satchler's surface vibration FF (solid line), and with a δ' FF (dashed line), and indirectly through the 2_1^+ level with a δ' FF (dotted line).

teron inelastic scattering data taken [33] in München at one sample angle (29°) with a resolution sufficient to resolve the 2_3^+ and 0_2^+ levels. The yield of the 0_2^+ level has been found to be approximately one sixth of that of the 2_3^+ state at that angle. The experimental data for the 2_3^+ state are compared with the theoretical calculations obtained by using only first-derivative form factors [see the dotted lines in Figs. 3–5]. Good fits have been obtained only for the deuteron data. The addition of a δ'' FF, with opposite sign with respect to that of the δ' one, improves the fits for all three probes [see the solid (S) and dashed lines (D) in Figs. 3–5].

The 2_4^+ data are reasonably reproduced by using the δ' FF's (dotted lines). At backward angles, contributions from the unresolved 6_1^+ level are expected. The 6_1^+ state is presumably excited by two-step processes through the 4_1^+ , 4_2^+ , and 2_1^+ levels. The largest $L=2$ contribution through the 4_2^+ state was found to be small even at backward angles when we evaluated its contribution using the β value de-

duced from the γ decay experiment. An $L=4$ contribution through the 2_1^+ level improves the fit for the 2_4^+ state as shown by solid (S) and dashed (D) lines in Figs. 3–5.

The 2_5^+ data from the three probes are satisfactorily reproduced by using δ' FF's. The results are also shown by the solid (S) and dashed (D) lines in Figs. 3–5.

The 2_7^+ analyzing power data from the 65 MeV proton experiment require a δ'' contribution in the direct excitation. For 400 MeV protons, no satisfactory fit could be achieved even when we tried to employ sign combinations of the β 's different from those required by 65 MeV proton and 56 MeV deuteron data. A possible reason could be due to the poor quality of the data.

C. Fits of 4^+ data

The 4_2^+ level is the most strongly excited one among the hexadecapole states. It is nicely fitted by only a direct δ' FF [see the solid (S) and dashed (D) lines in Fig. 6]. Indirect contributions are extremely weak and have not been included in the calculations because the fits are not significantly improved.

The angular distributions for the 4_1^+ state are different in shape from those for the 4_2^+ level. Hexadecapole direct δ' FF calculations are completely out of phase with respect to the data. When we take into account a δ'' FF direct contribution in the calculations, the 400 MeV cross section is well reproduced, but negative analyzing powers are predicted at backward angles for the 65 MeV data. The addition of an indirect contribution for the 4_1^+ excitation is sufficient to give good fits for all the data [solid (S) and dashed (D) lines in Fig. 6]. Based on this analysis, the 4_1^+ level is concluded to be mostly a pure $E2-E2$ two-quadrupole-phonon state.

IV. TRANSITION MATRIX ELEMENTS

The mass transition matrix elements are derived from the coupling constants β 's by using the expression

$$M^{(i)}(E\lambda) = \frac{A}{2} \beta_\lambda^{(i)} \frac{\int V_{\text{tr}}(r) r^\lambda d\tau}{\int V(r) d\tau}, \quad (1)$$

where (i) refers to the probe, (p, p') or (d, d') reactions. The reduced transition probabilities are obtained from the matrix elements by using the expression

$$B^{(i)}(E\lambda, J_i \rightarrow J_f) = \frac{|M^{(i)}(E\lambda)|^2}{(2J_i + 1)}. \quad (2)$$

The M values obtained by using Eq. (1) for the three probes and for the two (S and D) formalisms are listed in Table III. The quoted errors include only the β correlation errors from Table II and those on the NF values from Table I. These errors, mainly due to data analysis, usually dominate over statistical and systematical ones, except in the few cases of very good fits to the experiment.

No error has been included for the absolute value of the cross sections (UNF), because the extracted M 's are somewhat insensitive to it; in fact these quantities are determined mainly by the ratio [see Eq. (1)] of inelastic to elastic cross sections.

TABLE III. Multipole matrix elements (in $e \text{ fm}^\lambda$) for the lowest possible multipoles ($\lambda \geq 2$) for the indicated transitions, formalisms (S, D), and for the three probes (p, d, p_{400}), deduced from Table II and Eq. [1]. The quoted errors include the correlation errors from Table I and the NF uncertainties in Table I.

$J_{\text{in}}^\pi - J_{\text{fin}}^\pi$	$M^{(p,S)}$	$M^{(d,S)}$	$M^{(p_{400},S)}$	$M^{(p,D)}$	$M^{(p_{400},D)}$
$0_{\text{g.s.}}^+ - 2_1^+$	38.0 ± 1.2	36.2 ± 2.1	28.7 ± 2.9	37.5 ± 1.0	34.4 ± 2.2
$2_1^+ - 2_1^+$	32.3 ± 11.7	36.0 ± 15.8	25.4 ± 13.9	31.1 ± 9.7	27.2 ± 12.2
$0_{\text{g.s.}}^+ - 3_1^-$	163.4 ± 9.2	141.5 ± 8.7	124.8 ± 7.5	137.9 ± 7.2	143.8 ± 10.3
$0_{\text{g.s.}}^+ - 2_2^+$	10.2 ± 1.0	8.0 ± 1.5	6.2 ± 0.8	9.3 ± 0.5	7.4 ± 0.9
$2_1^+ - 2_2^+$	45.2 ± 3.6	35.6 ± 10.3	31.1 ± 13.3	24.5 ± 6.9	34.0 ± 10.6
$0_{\text{g.s.}}^+ - 2_3^+$	2.0 ± 0.7	1.2 ± 0.7	3.7 ± 0.7	2.5 ± 0.5	4.2 ± 0.4
$2_1^+ - 2_3^+$	21.3 ± 7.2	17.4 ± 8.9	12.5 ± 7.8	9.7 ± 6.3	13.5 ± 6.5
$0_{\text{g.s.}}^+ - 2_4^+$	8.9 ± 0.8	6.1 ± 0.7	8.7 ± 0.6	8.3 ± 0.4	10.2 ± 0.8
$2_1^+ - 2_4^+$	12.7 ± 5.2	13.8 ± 7.9	11.6 ± 7.5	12.7 ± 5.8	16.2 ± 13.8
$2_1^+ - 6_1^+$	1849 ± 464	1855 ± 466	1378 ± 348	1610 ± 403	1706 ± 435
$0_{\text{g.s.}}^+ - 2_5^+$	7.8 ± 0.5	5.5 ± 0.7	6.0 ± 0.8	7.2 ± 0.4	7.0 ± 0.6
$2_1^+ - 2_5^+$	7.0 ± 4.4	8.5 ± 5.9	11.8 ± 9.4	7.3 ± 3.5	9.7 ± 10.8
$0_{\text{g.s.}}^+ - 2_7^+$	4.4 ± 0.9	4.1 ± 0.7	1.9 ± 0.8	4.8 ± 0.7	2.3 ± 0.9
$2_1^+ - 2_7^+$	35.2 ± 21.0	12.4 ± 5.4	76.5 ± 16.4	14.1 ± 8.3	93.2 ± 20.0
$0_{\text{g.s.}}^+ - 4_1^+$	232 ± 58	214 ± 39	144 ± 20	185 ± 27	170 ± 26
$2_1^+ - 4_1^+$	78.7 ± 21.0	61.9 ± 4.5	67.4 ± 8.2	65.1 ± 6.8	96.3 ± 15.6
$0_{\text{g.s.}}^+ - 4_2^+$	581 ± 35	492 ± 47	406 ± 22	439 ± 22	469 ± 32

A modification of Eq. (1), with the atomic mass Z instead of $A/2$ in Eq. (1), defines the ‘‘modified’’ version of the elements which are often used [28] to compare transition rates deduced from hadron scattering with those from electromagnetic (em) measurements. The comparison of the matrix elements obtained from the three probes is reported in Fig. 9. The matrix elements for the direct excitations from the $0_{\text{g.s.}}^+$ state to the six 2^+ states and to the 4_1^+ , 4_2^+ , and 3_1^- states are presented in the top part of the figure. The matrix elements for their two-step excitations from the 2_1^+ level are also presented in the bottom part. The M values from the em experiments are shown with the solid circles. The M values obtained from our work are shown with the squares, and downward pointing and upward pointing triangles, for 65 MeV protons (p), 56 MeV deuterons (d), and 400 MeV protons (p_{400}), respectively. The results from the S and D formalisms are shown by the solid and open symbols, respectively. The corresponding S and D matrix elements agree with each other within errors in most of the cases. But for the experimental data at $E_p=400$ MeV, the S matrix elements are always lower than the D ones, while an opposite situation, with smaller differences, is shown by the squares in Fig. 9 for the 65 MeV proton values. The M values for a given transition, slightly displaced on the x axis according to increasing sensitivity of the probe to target protons, show an approximately linear trend with negative slopes which indicate that the analyses of these data allow the detection of the isovector components.

The two-step values of the three hadron probes, which are shown in the bottom part of Fig. 9, are more scattered than the direct ones. This reflects the fact that a reliable determination of two-step matrix elements is difficult. In general, their uncertainties are larger than those from em experiments (solid circles), in contrast with those in the upper part of the figure. These larger errors are probably due, as anticipated, to the adoption of a simplified coupling scheme, the omission

of the reorientation terms, and the reduced oscillation pattern of indirect contributions compared to the direct ones.

For a more detailed comparison of the transition matrix elements derived by the different probes, Eq. (1) is subdivided into neutron and proton components and, furthermore, into dynamic and static parts. Denoting $b_{p(n)}^{(i)}$ as the normalized ($b_p^{(i)} + b_n^{(i)} = 1$) interaction strengths of the i probe with the target neutrons and protons, and $M_{p(n)}$ as the proton (neutron) matrix elements, we have

$$M^{(i)}(E\lambda) = b_p^{(i)} M_p + b_n^{(i)} M_n. \quad (3)$$

The b_n/b_p values are assumed to be proportional to the volume integrals of the central isoscalar and isovector potentials $(V_0 + V_\tau)/(V_0 - V_\tau)$. $M_{p(n)}$ are linked to the transition operators Q_p and Q_n , which are evaluated by nuclear models, through the polarization charges e_p and e_n :

$$M_{p(n)} = e_{p(n)} Q_p + e_{n(p)} Q_n. \quad (4)$$

The isoscalar and isovector matrix elements are obtained as

$$M_s = \frac{M_n + M_p}{2}, \quad (5)$$

$$M_v = \frac{M_n - M_p}{2}. \quad (6)$$

For electric transitions, an em probe like the (e, e') scattering or γ decay is only sensitive to the proton transitions $b_p^{(\text{em})} = 1$, $b_n^{(\text{em})} = 0$. The inelastic scattering of low-energy protons and of 200 MeV negative pions [1] has the maximum sensitivity to neutron transitions $b_n^{(p)} = 0.75$, $b_p^{(p)} = 0.25$. Inelastic scattering of isoscalar particles like deuterons or alphas has equal sensitivity to neutron and proton

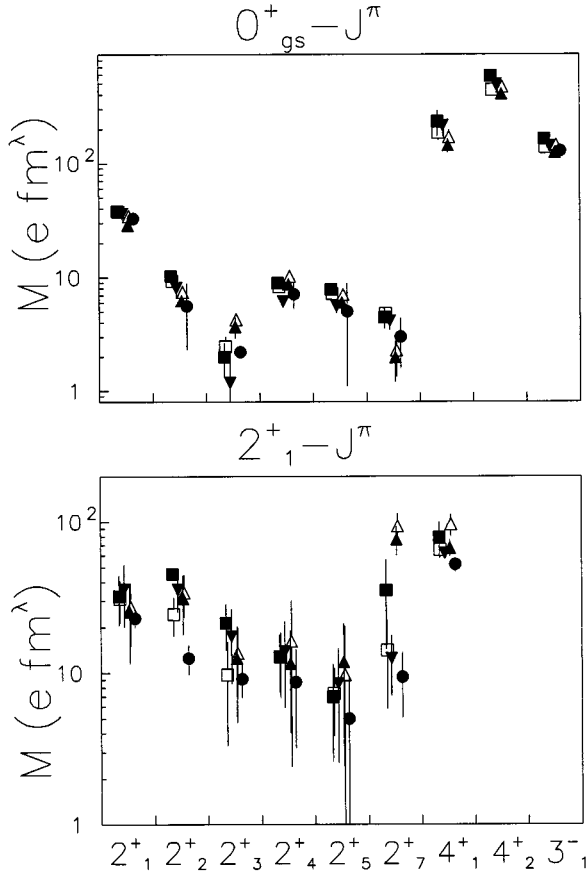


FIG. 9. Comparison of the multipole transition matrix elements for the indicated 2^+ , 4^+ , and 3^- states in ^{56}Fe . In the upper and lower parts, the direct (from the $0^+_{\text{g.s.}}$ state) and indirect (from the 2^+_1 state) matrix elements are shown, respectively. Squares, and downward pointing and upward pointing triangles stand for the values deduced from the scattering of 65 MeV protons, 56 MeV deuterons, and 400 MeV protons, respectively. The solid and open symbols correspond to the results from the Schrödinger and Dirac calculations, respectively. The solid circles for the 2^+ and 4^+_1 states are the values deduced from the transition matrix elements in the γ decay study of Ref. [9]. The solid circle for the 3^-_1 state is obtained in the (e, e') scattering work [10].

transitions $b_p^{(d)}=0.5$, $b_n^{(d)}=0.5$. The inelastic scattering of low-energy neutrons and of 200 MeV positive pions is mostly sensitive to proton transitions $b_p^{(n)}=0.75$, $b_n^{(p)}=0.25$. At higher energies, proton scattering decreases its sensitivity to neutron transitions. At 400 MeV, to our knowledge, there is no measurement of the volume integrals of the isoscalar and isovector parts in the OM potential. We assume these values from an effective nucleon-nucleon interaction derived from phenomenological nucleon-nucleon scattering amplitudes. By averaging the values in Fig. 1 of Ref. [34] and in Fig. 7 of Ref. [35], we get $b_n^{(p_{400})}=0.55$, $b_p^{(p_{400})}=0.45$. These values indicate that at 400 MeV proton scattering is mostly isoscalar. A 5% of uncertainty has been estimated for these $b_n^{(p_{400})}$ and $b_p^{(p_{400})}$ values and considered in the extraction of the $M_{p,n}$ matrix elements.

Equation (3) suggests that at least one pair of probes is needed to determine M_p and M_n . With the data from the three probes measured in this work ($M^{(p)}$, $M^{(d)}$, $M^{(p_{400})}$),

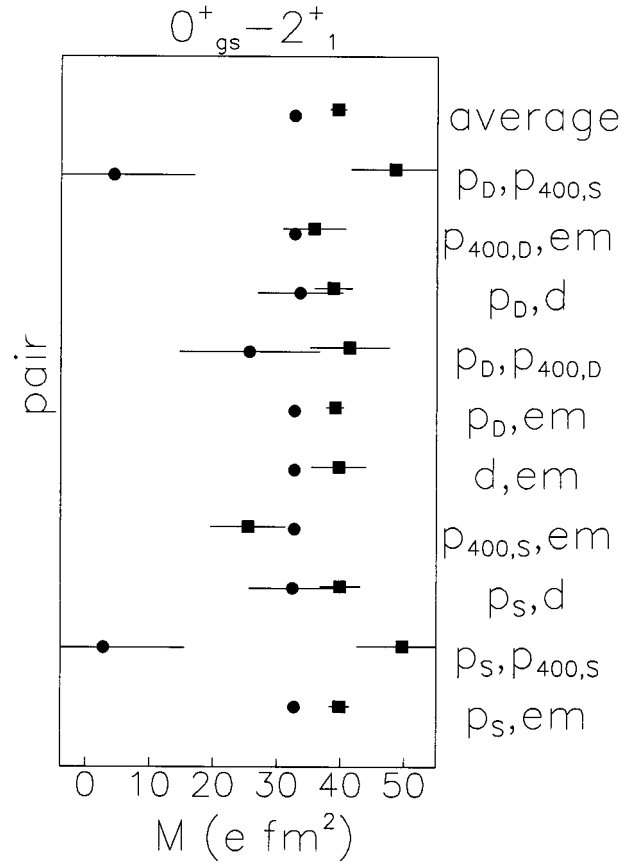


FIG. 10. The proton (M_p , circles) and neutron (M_n , squares) matrix elements for the $0^+_{\text{g.s.}}-2^+_1$ transition deduced from the indicated ten evaluations. The weighted average from all the evaluations is reported in the highest line.

and with the em values ($M^{(\text{em})}$) available in Refs. [9] and [10], we can determine M_p and M_n from six pairs. Best accuracy is obtained [1] by a pair in which one probe is mostly sensitive to proton transitions and the other to neutron transitions. Since pairs with nearly the same b_n/b_p ratio have a low sensitivity (which is proportional to the difference between the b_n/b_p values of the two probes), we disregard the determination of M_p and M_n from the pair $[p_{400}, d]$. In the order of decreasing sensitivity, the remaining five pairs are $[p, \text{em}]$, $[p_{400}, \text{em}]$, $[d, \text{em}]$, $[p, d]$, and $[p, p_{400}]$. The number of evaluations increases to 10 when we take into account the M ($M^{(p_S)}$, $M^{(p_D)}$, $M^{(d_S)}$, $M^{(p_{400,S})}$, $M^{(p_{400,D})}$) values from the two different formalisms (p_S , p_D , d_S , $p_{400,S}$, $p_{400,D}$).

Figure 10 shows the results from the ten evaluations of M_p and M_n for the most important $0^+_{\text{g.s.}}-2^+_1$ transition. Large deviations among the deduced M_p and M_n are found in pairs in which the $p_{400,S}$ probe is involved. The origin of these deviations arises from the imaginary potential (see Table I), which is the dominant term of the $p_{400,S}$ OM potential, and which is responsible for the low $M(E2)/\beta$ value in Table I compared to that of the p_S and d probes. This value, in spite of the highest β value observed by the p_{400} probe among the S evaluations, makes $M^{(p_{400,S})}$ very low and very near to the $M^{(\text{em})}$ value. Instead, the $M^{(p_{400,S})}$ value is expected to be nearly equal to the $M^{(d)}$ (reported as $M^{(d_S)}$ in Table III) one, since the isospin sensitivity is nearly equal for the p_{400} and d probes. The upper line of Fig. 10 shows the weighted

TABLE IV. Weighted averages for proton M_p and neutron M_n transition matrix elements (in $e \text{ fm}^\lambda$) for the lowest possible multipoles ($\lambda \geq 2$) for the indicated transitions. The values deduced from the following pairs of total matrix elements, $[M^{(p)}, M^{(\text{em})}]$, $[M^{(p_{400})}, M^{(\text{em})}]$, $[M^{(d)}, M^{(\text{em})}]$, $[M^{(p)}, M^{(d)}]$, and $[M^{(p)}, M^{(p_{400})}]$, have been included in the averages. The total matrix elements have been taken from Refs. [9,10] for the em probe, from the averages of the $M^{(p,S)}$ and $M^{(p,D)}$ values in Table III for the p probe, and from the $M^{(d_s)}$ and $M^{(p_{400},D)}$ values in Table III for the d and p_{400} probes, respectively.

$J_{\text{in}}^\pi - J_{\text{fin}}^\pi$	M_p	M_n
$0_{\text{g.s.}}^+ - 2_1^+$	32.7 ± 0.4	39.4 ± 0.9
$2_1^+ - 2_1^+$	23.0 ± 1.7	34.4 ± 7.8
$0_{\text{g.s.}}^+ - 3_1^-$	128.1 ± 8.9	158.1 ± 7.0
$0_{\text{g.s.}}^+ - 2_2^+$	4.7 ± 1.6	11.3 ± 0.9
$2_1^+ - 2_2^+$	12.6 ± 1.6	42.1 ± 4.5
$0_{\text{g.s.}}^+ - 2_3^+$	2.2 ± 0.1	2.6 ± 0.4
$2_1^+ - 2_3^+$	9.1 ± 1.3	17.6 ± 4.7
$0_{\text{g.s.}}^+ - 2_4^+$	6.5 ± 0.9	9.3 ± 0.6
$2_1^+ - 2_4^+$	8.9 ± 3.1	14.0 ± 4.5
$0_{\text{g.s.}}^+ - 2_5^+$	3.8 ± 1.3	8.9 ± 0.6
$2_1^+ - 2_5^+$	5.2 ± 2.6	7.8 ± 3.3
$0_{\text{g.s.}}^+ - 2_7^+$	2.8 ± 0.7	5.1 ± 0.6
$2_1^+ - 2_7^+$	9.5 ± 2.5	25.0 ± 8.1
$0_{\text{g.s.}}^+ - 4_1^+$	145 ± 94	226 ± 55
$2_1^+ - 4_1^+$	52.5 ± 3.1	76.6 ± 7.5
$0_{\text{g.s.}}^+ - 4_2^+$	409 ± 109	538 ± 52

averages of M_p and M_n for the 2_1^+ direct excitation. These averages are scarcely influenced by $M^{(p_{400,S})}$ because of its uncertainty.

The M_p and M_n weighted averages for all the transitions are reported in Table IV. The values obtained from the above reported five pairs of probes have been included in the averages. The means of the S and D determinations has been taken as p probe values $[M^{(p)} = (M^{(p,S)} + M^{(p,D)})/2]$, only the Dirac determination as p_{400} ones ($M^{(p_{400})} = M^{(p_{400,D})}$). The averaging of the obtained five M_p 's and M_n 's has been made by taking the inverse of the squared uncertainties as weights. The results are weakly affected when the $M^{(p_{400,S})}$ values are also used $[M^{(p_{400})} = (M^{(p_{400,S})} + M^{(p_{400,D})})/2]$, or when we assume different weights in the averages. This suggests that we can obtain rather reliable $M_{p,n}$ values by using several probes. The values for the quadrupole states given in Table IV are displayed by the solid circles in Fig. 11. This figure, which is subdivided in direct (left) and two-step (right side) values, displays the determined averages of M_p , M_n/M_p , and M_v/M_s . In the M_p part, the $M^{(\text{em})}$ values from Ref. [9] have been also reported with open triangles. The agreement between the M_p 's here deduced and the $M^{(\text{em})}$ values is generally good. The straight lines drawn in the second and third parts of Fig. 11 correspond to N/Z and to the ϵ asymmetry parameter, respectively. All the deduced M_n/M_p values lie above the N/Z line, indicating that neutron transition amplitudes dominate the excitation of the quadrupole states in ^{56}Fe . A similar behavior is observed for the M_v/M_s values with respect to the asymmetry line. The highest M_v/M_s value is around 0.4 for direct transitions, and is around 0.5 for two-step transitions.

The direct excitations of the 2_1^+ , 2_3^+ , and 2_4^+ levels are mostly isoscalar. Those of the 2_2^+ , 2_5^+ , and 2_7^+ states have an appreciable isovector component. The summed isovector quadrupole strength detected in all the six 2^+ states amounts

to $M_v \approx 12 e \text{ fm}^2$, the isoscalar to $M_s \approx 64 e \text{ fm}^2$. Among two-step processes, only the 2_2^+ and 2_7^+ excitations have an isovector contribution.

From this analysis we suggest that the quadrupole mixed-symmetry strength in ^{56}Fe is split among the 2_2^+ , 2_5^+ , and 2_7^+ states. The M_v isovector strength in these states is 20% of the M_s isoscalar strength of the symmetric 2_1^+ state.

The M_v/M_s ratio for the 3_1^- , 4_1^+ , and 4_2^+ levels is 0.10 ± 0.04 , 0.19 ± 0.07 , and 0.14 ± 0.13 , respectively. These values are weak and similar to that of the 2_1^+ level. Thus, it is concluded that the excitations of the most strongly excited states of ^{56}Fe with low multipolarities are due to isoscalar transitions.

V. MODEL CALCULATIONS OF TRANSITION MATRIX ELEMENTS

The transition matrix elements discussed in the previous paragraph and their isovector contents are compared with the predictions from the shell model [8] and from the IBA-2 model [11].

The shell model calculation by Nakada *et al.* [8] assumes ^{40}Ca as a doubly magic inert core, and considers the following configurations: $(0f_{7/2})^{14-k} (0f_{5/2}1p_{3/2}1p_{1/2})^{2+k}$ with $k=0,1$, and 2. The $k=2$ configuration, which results in a large configuration space, has been found to play an essential role in considering the effects of pairing and deformation. The spectrum of ^{56}Fe resulting from this calculation is reported in Fig. 12 along with the experimental energies of the studied levels and of the first states of other positive multipolarities. The excitation energies of 2^+ levels are quite well reproduced at least up to the 2_6^+ state. The electric transition properties are deduced in Ref. [8] by assuming the ratio $e_\pi/e_\nu=1.56$ for the quadrupole effective single-particle charges. The calculated values (open circles) are compared

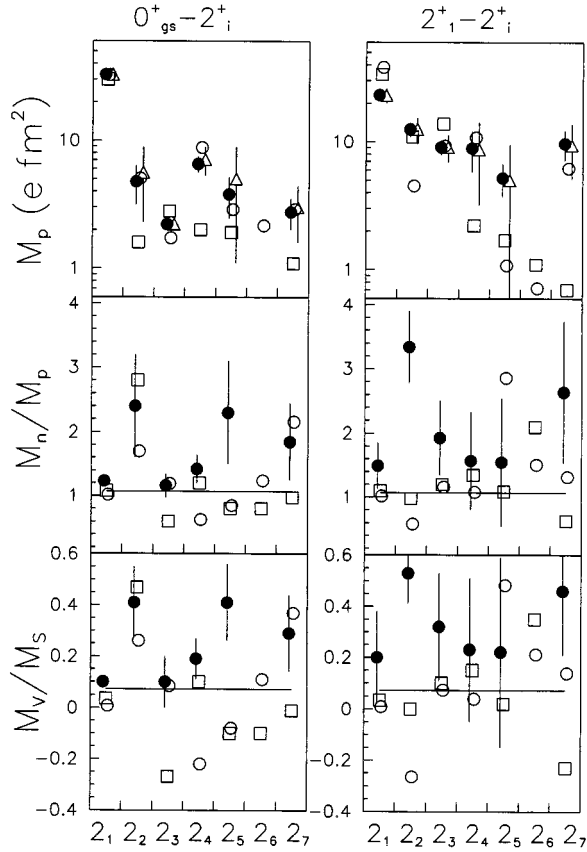


FIG. 11. The proton transition matrix elements (M_p), the ratios of neutron to proton matrix elements (M_n/M_p), and the ratios of isovector to isoscalar (M_v/M_s) quadrupole matrix elements. Those for the direct (left part) and indirect (right part) excitation of the 2^+ states in ^{56}Fe are displayed. Weighted average values deduced in this paper are reported with the solid circles. Values from the γ -decay work [9] are shown with the open triangles. The open squares are the predictions from Ref. [11] in the IBA-2 model. The shell-model calculations of Ref. [8] are given by the open circles.

to the experimental values (solid circles) in Fig. 11. The calculated direct M_p 's are very near to the experimental values, showing a good reproduction of the proton part of the transitions. The calculated values for M_n/M_p and M_v/M_s suggest that there is an isovector content in the direct exci-

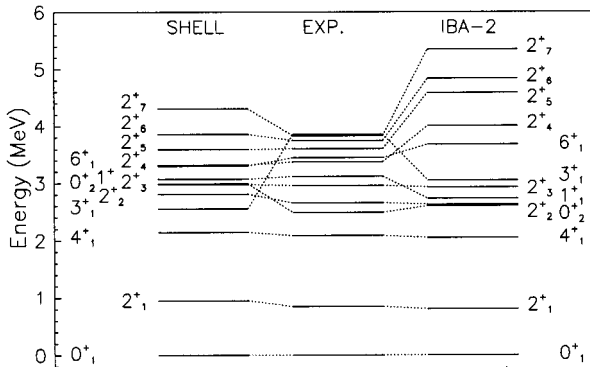


FIG. 12. Experimental excited levels in ^{56}Fe and those calculated in the framework of the IBA-2 and shell models.

tation of the 2_2^+ , 2_4^+ , 2_5^+ , and 2_7^+ levels. These findings mostly agree with our experimental results except for the 2_4^+ state. However, the signs of the isovector parts for the direct excitation of the 2_5^+ level and of the 2_2^+ indirect one are opposite to the results of the present analysis.

The IBA-2 calculations of Rikovska and Stone [11] deal with the even isotopes of iron from $A=56$ to 62. The closure $N=Z=28$ (^{56}Ni) is not considered for the severe truncation to the boson space, since the configuration space allowed is too small to predict all the 2^+ states here analyzed. The ^{48}Ca closure is instead assumed which allows for three proton particle bosons for ^{56}Fe instead of the one proton-hole boson in the $f_{7/2}$ shell orbit, leaving all the neutrons in the $pf_{7/2}$ shell orbits. The IBA-2 Hamiltonian parameters calculated in Ref. [11] depict ^{56}Fe very close to the SU(3) limit for the deformed rotor nuclei. These parameters are reported here, for convenience, in the usual notation: $\epsilon=1.32$, $k=-0.36$, $\chi_\nu=-1.3$, $\chi_\pi=-1.2$, $c_{(0,2,4)\nu}=0.0,0.0,0.0$, $c_{(0,2,4)\pi}=0.9,0.6,0.1$, $\chi_1=\chi_3=-0.26$, $\chi_2=0.13$. The comparison between experimental and calculated energy levels (Fig. 12) suggests that only the three lowest 2^+ states are well reproduced. The excitation energies of higher 2^+ states are overestimated. From the states above the 2_4^+ level it is moreover difficult to get the correspondence between calculated and observed levels. The em properties have been evaluated in Ref. [11] by assuming $e_\pi/e_\nu=1$ for the quadrupole effective boson charges. A value $e_\pi/e_\nu=1.6$ was assumed in Ref. [6] for the analysis of the first three 2^+ charge transition densities of ^{56}Fe . A higher value of $e_\pi/e_\nu=1.9$ is determined in Ref. [36] if the SU(3) limit is assumed for ^{56}Fe , and from the formula $e_\pi/e_\nu=(M_n N_n - M_p N_p)/(M_p N_n - M_n N_p)$ in Ref. [37]. These values result in strong isovector contents, which are not consistent with our experimental results. A lower value $e_\pi/e_\nu=1.2$ has been found to give a sufficient description of the M_p 's for the first three 2^+ states and of the M_v/M_s values of the 2_1^+ , 2_2^+ , and 2_4^+ levels (open squares in Fig. 11).

VI. CONCLUSIONS

The results of the inelastic scattering of polarized protons at 65 and 400 MeV and of deuterons at 56 MeV, leading to the excitation of low-lying states in ^{56}Fe , have been presented. Scattered particles have been magnetically analyzed. For 400 MeV protons, good energy resolution has been achieved by the newly constructed magnetic spectrometer "Grand Raiden."

Experimental data have been described by the CC calculations within the Schrödinger and Dirac formalisms. Deformed OM transition potentials derived by adding first- and second-derivative form factors have been used. The approach has been shown to satisfactorily reproduce the cross sections and analyzing powers of the transitions for each of the three probes investigated. The δ'' contribution is necessary in the analysis of the 2_2^+ , 2_3^+ , 2_7^+ , and 4_1^+ data. It is added to the δ' contribution with a different sign for the 2_2^+ and 2_3^+ cases, while it is the only necessary contribution for the direct excitation of the 4_1^+ level.

From these analyses, the transition matrix elements $M(E\lambda)$ have been deduced and compared among them-

selves. The $M(E\lambda)$ values extracted from the 400 MeV proton data using the Schrödinger formalism are lower than those derived from the other probes. The Dirac formalism predicts higher $M(E\lambda)$ values than the Schrödinger one at 400 MeV, but slightly lower at 65 MeV. The energy dependence of $M(E\lambda)$ from the Schrödinger potentials, first observed in Ref. [15], deserves more careful investigation. Moreover, one would like to understand to which extent the $M(E\lambda)$'s deduced from Dirac potentials are energy independent.

The comparison of the $M(E\lambda)$'s deduced in this paper from the data obtained with the three probes to those from γ decays or (e, e') scattering has been used to deduce the neutron and proton components of the matrix elements. In particular, the isospin character of the excitations of six 2^+ levels has been determined. The 2_3^+ level, which shows an angular dependence different in shape from that of the other quadrupole states, is excited by isoscalar transitions. Isoscalar are also the transitions leading to the 2_4^+ state. The direct excitations of the 2_2^+ , 2_5^+ , and 2_7^+ levels contain an appreciable isovector component. These levels share 60% of the detected quadrupole, isovector strength M_v . The most strongly excited quadrupole, octupole and hexadecapole states (2_1^+ , 3_1^- , and 4_2^+) in ^{56}Fe have isoscalar characters.

The M_n/M_p and M_v/M_s values extracted in this work for the quadrupole transitions have been compared with IBA-2

and shell-model calculations. It has been found that both models correctly predict the isospin character of the direct excitation of the 2_1^+ and 2_2^+ levels, but fail for many of the other quadrupole transitions.

Our findings about the location of the quadrupole mixed-symmetry strength in ^{56}Fe agree with those of Refs. [5–7] only for the 2_2^+ level. Some discrepancies have been found for the location of other levels with weaker mixed-symmetry strengths. These differences indicate the difficulties to locate the mixed-symmetry strength in nuclei near to the SU(3) limit, where this excitation mode is supposed [2] to be weaker with respect to nuclei near to the O(6) limit. For a better understanding of the mixed-symmetry mode in the $A \approx 60$ mass region, the experimental determination of M_n/M_p for the quadrupole states in the neighboring nuclei of ^{56}Fe would be extremely useful.

ACKNOWLEDGMENTS

The authors like to thank N. Hama for helpful suggestions on Dirac calculations, H. Nakada for information on the shell model calculations, and G. Graw for the $^{56}\text{Fe}(d, d')$ spectrum taken at $E_d=20$ MeV. One of us (R.D.L.) acknowledges the hospitality received at RCNP during his stay in Osaka where most of the present calculations were done.

-
- [1] A.M. Bernstein, V.R. Brown, and V.A. Madsen, *Phys. Rev. Lett.* **42**, 425, 1979; *Phys. Lett. B* **103**, 255 (1981); **106**, 259 (1981).
- [2] F. Iachello, *Phys. Rev. Lett.* **53**, 1427 (1979).
- [3] A. Arima and F. Iachello, *Ann. Phys. (N.Y.)* **111**, 201 (1978).
- [4] M. Pignanelli, S. Micheletti, N. Blasi, R. De Leo, W.T.A. Borghols, J.M. Schippers, S.Y. van der Werf, and M.N. Harakeh, *Phys. Lett. B* **202**, 470 (1988); R. De Leo, L. Lagamba, N. Blasi, S. Micheletti, M. Pignanelli, M. Fujiwara, K. Hosono, I. Katayama, N. Matsuoka, S. Morinobu, T. Noro, S. Matsuki, H. Okamura, J.M. Schippers, S.Y. van der Werf, and M.N. Harakeh, *Phys. Lett. B* **226**, 5 (1989).
- [5] S.A.A. Eid, W.D. Hamilton, and J.P. Elliott, *Phys. Lett. B* **166**, 267 (1986).
- [6] G. Hartung, A. Richter, E. Spamer, H. Woertche, C. Rangacharyulu, C.W. de Jager, and H. de Vries, *Phys. Lett. B* **221**, 109 (1989).
- [7] H. Nakada, T. Otsuka, and T. Sebe, *Phys. Rev. Lett.* **67**, 1086 (1994).
- [8] H. Nakada, T. Sebe, and T. Otsuka, *Nucl. Phys.* **A571**, 467 (1994).
- [9] L.K. Peker, *Nucl. Data Sheets* **61**, 189 (1990).
- [10] R.H. Spear, *At. Data Nucl. Data Tables* **42**, 55 (1989).
- [11] J. Rikovska and N.J. Stone, in *Proceedings of Symmetries and Nuclear Structure*, Dubrovnik 1986, edited by R. A. Meyer and V. Paar (Harwood Academic, Chur, Switzerland, 1986), p. 122.
- [12] M. Pignanelli, N. Blasi, S. Micheletti, R. De Leo, L. Lagamba, R. Perrino, J.A. Bordewijk, M.A. Hofstee, J.M. Schippers, S.Y. van der Werf, J. Wesseling, and M.N. Harakeh, *Nucl. Phys.* **A540**, 27 (1992).
- [13] M. Pignanelli, N. Blasi, J.A. Bordewijk, R. De Leo, M.N. Harakeh, M.A. Hofstee, S. Micheletti, R. Perrino, V. Yu. Ponomarev, V.G. Soloviev, A.V. Sushkov, and S.Y. van der Werf, *Nucl. Phys.* **A559**, 1 (1993); R. Perrino, N. Blasi, R. De Leo, M.N. Harakeh, C.W. de Jager, S. Micheletti, J. Mieremet, M. Pignanelli, V.Yu. Ponomarev, R.K.J. Sandor, and H. de Vries, *ibid.* **A561**, 343 (1993).
- [14] J.R. Beene, D.J. Horen, and G.R. Satchler, *Phys. Lett. B* **344**, 67 (1995).
- [15] N.M. Hintz, D. Cook, M. Gazzaly, M.A. Franey, M.L. Barlett, G.W. Hoffmann, R. Fergerson, J. McGill, G. Pauletta, R.L. Boudrie, J.B. McClelland, and K.W. Jones, *Phys. Rev. C* **37**, 692 (1988).
- [16] H. Ikegami, S. Morinobu, I. Katayama, M. Fujiwara, and S. Yamabe, *Nucl. Instrum. Methods* **175**, 335 (1981).
- [17] Y. Fujita, K. Nagayama, M. Fujiwara, S. Morinobu, T. Yamazaki, and H. Ikegami, *Nucl. Instrum. Methods* **217**, 441 (1983).
- [18] J. Takamatsu, T. Nakagawa, A. Terakawa, A. Narita, T. Tohei, M. Fujiwara, S. Morinobu, I. Katayama, H. Ikegami, K. Katori, S.I. Hayakawa, Y. Fujita, M. Tosaki, and S. Hatori, *J. Phys. (Paris) Colloque* **51**, C6-423 (1990).
- [19] M. Fujiwara *et al.*, in *Proceedings of the International Symposium on Heavy Ion Research with Magnetic Spectrographs*, edited by N. Anantaraman and B. Sherrill, NSCL Technical Report No. MSUCL-685, 1989, p. 283.
- [20] T. Noro *et al.*, RCNP Annual Report, 1991, p. 177.
- [21] J. Raynal, computer program ECIS88, in *Workshop on Applied Theory and Nuclear Model Calculation for Nuclear Technology Applications (JCTP)*, Trieste, 1988.

- [22] S. Hama, B.C. Clark, E.D. Cooper, H.S. Sherif, and R.L. Mercer, *Phys. Rev. C* **41**, 2737 (1990); E.D. Cooper, S. Hama, B.C. Clark, and R.L. Mercer, *ibid.* **47**, 297 (1993).
- [23] S. Shim, B.C. Clark, E.D. Cooper, S. Hama, R.L. Mercer, L. Ray, J. Raynal, and H.S. Sherif, *Phys. Rev. C* **42**, 1592 (1990); L. Kurth, B.C. Clark, E.D. Cooper, S. Hama, S. Shim, R.L. Mercer, L. Ray, and G.W. Hoffmann, *ibid.* **49**, 2086 (1994); R. de Swiniarski, C. Glashausser, K. Jones, and D.L. Pham, *ibid.* **52**, 1110 (1995).
- [24] F. Ballester, E. Casal, and J.B.A. England, *Nucl. Phys.* **A501**, 301 (1989).
- [25] T. Noro, H. Sakaguchi, M. Nakamura, K. Hatanaka, F. Ohtani, H. Sakamoto, and S. Kobayashi, *Nucl. Phys.* **A366**, 189 (1981).
- [26] W.W. Daehnick, J.D. Childs, and Z. Vrcelj, *Phys. Rev. C* **21**, 2253 (1980).
- [27] K.W. Jones, C. Glashausser, R. de Swiniarski, S. Nanda, T.A. Carey, W. Cornelius, J.M. Moss, J.B. McClelland, J.R. Comfort, J.L. Escudie, M. Gazzaly, N. Hintz, G. Igo, M. Haji-Saeid, and C.A. Whitten, Jr., *Phys. Rev. C* **33**, 17 (1986).
- [28] M. Pignanelli, N. Blasi, S. Micheletti, R. De Leo, M.A. Hofstee, J.M. Schippers, S.Y. van der Werf, and M.N. Harakeh, *Nucl. Phys.* **A519**, 567 (1990).
- [29] V.G. Soloviev, *Z. Phys. A* **334**, 143 (1989); V.G. Soloviev and N.Yu Shirikova, *ibid.* **334**, 149 (1989).
- [30] R. De Leo, M. Pignanelli, W.T.A. Borghols, S. Brandenburg, M.N. Harakeh, H.J. Lu, S.Y. van der Werf, C.W. de Jager, J.B. van der Laan, and H. de Vries, *Phys. Lett. B* **162**, 1 (1990), and references therein.
- [31] G.R. Satchler, *Nucl. Phys.* **A100**, 481 (1967); *Part. Nucl.* **5**, 107 (1972).
- [32] M. Pignanelli, S. Micheletti, R. De Leo, S. Brandenburg, and M.N. Harakeh, *Phys. Rev. C* **33**, 40 (1986).
- [33] G. Graw (private communication).
- [34] M.A. Franey and W.G. Love, *Phys. Rev. C* **31**, 488 (1985).
- [35] P. Petrovich and W.G. Love, *Nucl. Phys.* **A354**, 499c (1981).
- [36] W.D. Hamilton, A. Irbach, and J.P. Elliott, *Phys. Rev. Lett.* **53**, 2469 (1984); S. Pittel and O. Scholten, *Phys. Rev. C* **38**, 555 (1988); J.N. Ginocchio and P. Van Isacker, *ibid.* **33**, 365 (1986).
- [37] R. De Leo, N. Blasi, S. Micheletti, M. Pignanelli, M.N. Harakeh, W.T.A. Borghols, J.M. Schippers, and S.Y. van der Werf, *Phys. Lett. B* **226**, 202 (1989).